Title page

Bridge Damage Detection using Precise Vision-based Displacement Influence Lines and Weigh-in-motion Devices: Experimental Validation

Authors: Liangfu Ge[1,a], Ki Young Koo[3,b], Miaomin Wang[4,c], James Brownjohn[3,d], Danhui Dan[1,2,*]

Affiliations:

1 School of Civil Engineering, Tongji University, 1239 Siping Road, Shanghai, 200092, China;

2 Key Laboratory of Performance Evolution and Control for Engineering Structures of Ministry of Education, Tongji University, 1239 Siping Road, Shanghai, 200092, China;

3 Vibration Engineering Section, College of Engineering, Mathematics and Physical Sciences, University of Exeter, Exeter EX4 4QJ, UK.

4 Faculty of Infrastructure Engineering, Dalian University of Technology, Dalian, 116024,China

*** Corresponding author, Professor. Email: dandanhui@tongji.edu.cn**

- ✓ **Mail Address:** *Room 711, Bridge Building, Tongji University, 1239 Siping Road, Shanghai, PR China;*
- ✓ **Mobile:** *86-13918075836*; **Fax:** *86-21-55042363*

Coauthor email:

a: liangfu@tongji.edu.cn; b: k.y.koo@exeter.ac.uk; c: wangmiaomin@mail.dlut.edu.cn; d: j.brownjohn@exeter.ac.uk

Acknowledgement: This study is financially supported by the Fundamental Research Funds for the Central Universities (20210205), the Zhejiang Zhoushan Sea-crossing Bridge Co Ltd. in the project “Vortex Vibration Prediction Technology of Xihoumen Bridge”, the China Railway Siyuan Survey and Design Group Co., Ltd. in the project "Research on the Target System and Index Algorithm of Urban Cluster Bridge Monitoring" (2020K-006-1), the National Natural Science Foundation of China(51878490), and the CSC (China Scholarship Council) Scholarship (202006260246).

Bridge Damage Detection using Precise Vision-based Displacement Influence Lines and Weigh-in-motion Devices: Experimental Validation

Abstract

This study presents an experimental validation for a high-precision vision-based Displacement Influence Line (DIL) measurement system for a purpose of damage detection on bridges. The vision-based DIL measurement system is a promising tool for structural health monitoring on real operation bridges, which combines two Computer Vision subsystems and weigh-in-motion (WIM) devices. Two vision systems are utilized for tracking vehicle position and measuring structural displacement, while the WIM device obtains vehicle weight information. To demonstrate the feasibility of such a vision-based DIL measurement system, this study developed a vision system using a Go-Pro camera for vehicle positioning and a consumer grade camera for displacement measurement, followed by a series of laboratory experiments on a simply supported bridge using vision-based DILs to assess damage existence and localisation. Five damage scenarios were created by restrengthening the test structure instead of damaging it. Each restrengthened structure was considered intact while the original structure was considered damaged. Vision-based DIL measurements were repeated 12 times for each damage scenario to observe uncertainties in damage localisation as well as DILs. As the measured DILs were found adversely affected by the friction on the boundary supports, the Chordwise Displacement Influence Line (cw-DIL) approach

was proposed to compensate for this effect. Damage-induced cw-DILs were shown to be able to assess damage existence and localisation successfully and consistently for all five damage scenarios.

Keywords: bridge damage detection, vision-based measurement, vehicle-induced displacements, influence line, changeable load speed.

1 Introduction

The progressive deterioration of bridges is one of the major concerns for bridge owners. In order to ensure structural safety and cost-effective maintenance of bridges, it is important to develop technologies to identify structural deterioration or damage ideally at an early stage.

Structural health monitoring and damage detection for bridges have been a long endeavour in structural engineering for more than four decades (Doebling et al. 1996; Sohn et al. 2002; Das et al. 2016; Han et al. 2021). Most of the efforts were using output-only measurements such as acceleration, strain, displacement, tilt, etc, mainly due to their relative easiness to measure, and showed different levels of success in numerical and lab experimental studies. To the best knowledge of the authors, there is no methodology validated to be effective on real operational bridges. There were two common barriers to such validation: 1) the measured quantities required by the developed methodologies were influenced not only by damage, but also by ambient environmental changes such as vehicle volume (Cross et al. 2013; K.-Y. Koo et al. 2013), thermal effect (de Battista et al. 2015; Han et al. 2021), and wind loading

(Brownjohn et al. 1994; Dan et al. 2022), and 2) more importantly it was extremely challenging to make artificial damage or an equivalent effect on real operational bridges.

Beyond the output-only approaches, an alternative approach was to measure the changes of bridge influence lines (ILs) with both input and output information. An early attempt was using video recording to identify vehicles and strain sensors on the bridge to produce strain influence lines (SILs) (Zaurin and Catbas 2009), which were later applied to damage detection in a bridge model (Zaurin and Catbas 2011). Also, the displacement influence line (DIL) has been recognised as another promising tool. Methodologies to use displacement influence lines were developed for damage localisation and quantification with studies on laboratory bridge models (He et al. 2017b; Chen et al. 2018; Le et al. 2019). There were variations in damage localisation methods: curvature based (He et al. 2017b), optimisation based (Chen et al. 2018), and displacement based (Le et al. 2019). There were also variations in damage quantification as well: solving a set of linear equations (He et al. 2017b), optimisation (Chen et al. 2018), and slope of displacement (Le et al. 2019). Rotational influence lines (RILs) were also considered an attractive tool for damage detection, especially around supports where DILs have a lower sensitivity to damage. A damage localisation method was proposed by finding an abrupt change in RILs (Yu Zhou et al. 2018), and experimental validations in the laboratory and field were carried out (Huseynov et al. 2020). To combine the advantages of DILs and RILs in damage detection, a method for the estimation of flexural bending rigidity was proposed with information from a FE

model and validated through a numerical simulation (Breccolotti and Natalicchi 2022).

To implement field measurements for DIL or RIL, it is highly promising to apply emerging computer vision technologies to measure vehicle trajectories and bridge displacements. Vision-based displacement measurement has been intensively studied in recent years (Xu et al. 2018; Lydon et al. 2019; Kromanis 2021). According to the size of the field of view, such measurement approaches can be implemented in two ways: single-point measurement (Kromanis 2021) and distributed measurement (Xu et al. 2018). The distributed measurement can yield more comprehensive structural information, however, laboratory and field trials showed that it is less precise than single-point measurements (Lydon et al. 2019). Correspondingly, distributed vision-based methods have also been applied to DIL measurements. Erdenebat and Waldmann (2020) used a full-frame camera to measure multi-point displacements along a concrete bridge under the loading of six controlled trucks. Lydon et al. (2021) proposed a roving camera technique to measure displacements at various positions along a bridge repeatedly loaded by the same vehicle. As these DIL measurement methods relied on the control of loading vehicles, some studies turned attention to integrating single-point displacement measurement with another vision system for vehicle position measurement. Dong et al. (2019) implemented a field DIL measurement system for a small real truss bridge. Martini et al. (2022) identified the DILs of a steel beam for finite element model updating. Such input-output vision systems have the potential to obtain DILs for operational bridges, however, there is little research on their applications for

damage detection, which imposes strict accuracy requirements on both displacement measurement and vehicle positioning. A recent work (Khuc and Catbas 2018) reported a successful detection of the damage existence in a steel bridge, however, the results of damage localisation were not entirely satisfactory and limited by the accuracy of vision systems. Therefore, it remains necessary to develop an input-output vision system with higher precision and study its performance on DIL-based damage detection.

Considering the above obstacles, this paper aims to propose a high-precision vision-based DIL measurement system and validate its feasibility for damage detection by performing laboratory experiments on a bridge model. The bridge model was not damaged but restrengthened so that the restrengthened structure was considered as the intact structure, whilst the original structure as a damaged structure. Moreover, the concept of integrating weigh-in-motion (WIM) with vision systems is introduced in this study, which offers the possibility for DIL-based damage detection to be repeatedly conducted on operational bridges by using different crossing vehicles.

The remainder of this paper is organised as follows. Section 2 introduces the theoretical basis of the vehicle position measurement, bridge displacement measurement, and the damage detection method using DILs. Section 3 provides the details of the experiments for the laboratory bridge model and the damage scenarios. Section 4 presents the measurements, constructed DILs, and the damage detection results, followed by Conclusion.

2 Theory

2.1 The Vision-based Damage Detection System

Vehicle loading is one of the three major loadings on bridges, i.e., vehicle loading, thermal loading and wind loading (especially for long-span bridges). In spite of the importance, it was practically difficult to measure the distribution of vehicle loading at a given time on a bridge. But due to the widespread technology of Computer Vision (CV), it has become feasible to measure it by integrating CV and a weigh-in-motion (WIM) system, as well as the structural response of a bridge. This change gave a rise of the idea to use computer vision for a purpose of structural health monitoring and damage detection.

Fig.1 shows an overview of the proposed vision-based damage detection system that uses damage-induced displacement influence lines. It includes two computer vision-based measurement systems and a WIM system. Vision subsystem A is responsible for measuring vehicle positions, while vision subsystem B monitors structural displacements. In addition, the WIM system records weight information for each passing vehicle. By properly synchronizing the subsystems and fusing the information from the three measurements for different vehicles, accurate displacement influence lines (DILs) can be generated. Usually, structural displacement measurements have dynamically oscillating components due to the natural frequencies, but a quasi-static component of them can be extracted by low-pass filtering with a proper cut-off frequency. Structural damage detection can be done using changes in the DILs before

and after damage. Although the proposed damage detection system assumes there is only one vehicle on the bridge during the time of DIL measurements, it can be applied to repeated measurements for vehicles of various weights so which enables implementation on operational bridges.

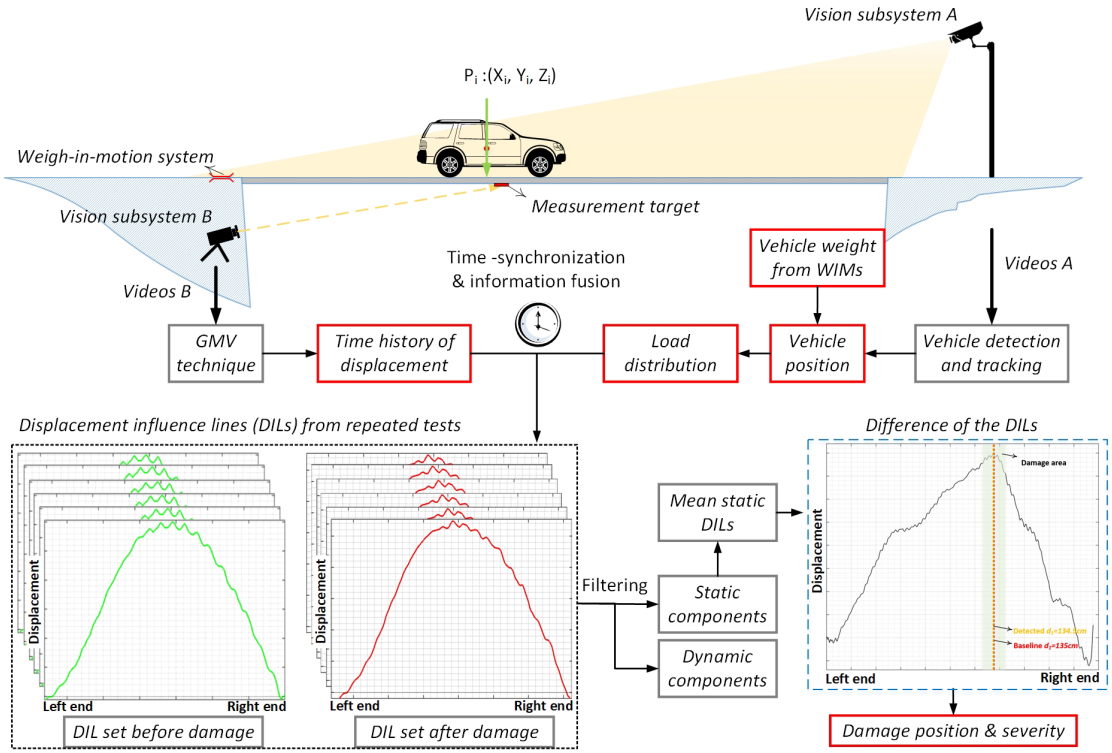

Fig.1 Overview of the proposed vision-based damage detection system

The theory of vehicle position measurement is described in Section 2.2 and that of structural displacement measurement is in Section 2.3. The DIL-based damage detection method is presented in Section 2.4.

2.2 Vehicle Position Measurement

Vehicle position measurement involves 1) "vehicle position identification" in the image coordinates for each frame of a video stream, and 2) transformation of the identified vehicle position from the image coordinates to the bridge deck coordinates.

Vehicle position identification refers to detecting and tracking a vehicle in image

sequences. In the existing studies on vision-based damage detection or DIL identification, vehicle position was identified by traditional algorithms such as the background difference (Zaurin and Catbas 2009; Zaurin and Catbas 2011; Zaurin et al. 2016; Chen et al. 2017) and optical flow (Dong et al. 2019). The traditional algorithms are faster in computation and easy to deploy, but are adversely affected by the change in illumination, limiting the accuracy of vehicle position measurement. Recently, with the rapid development of Deep Learning, a series of vehicle position identification algorithms have emerged based on CNN backbones and been proven to be highly accurate and robust in real bridge scenarios (Ge et al. ; Ge et al. 2020; Yun Zhou et al. 2020). This study used a YOLO-v4-based detection model and the Kalman filtering algorithm for vehicle detection and tracking, respectively. As a result, a bounding box of a vehicle is obtained in each frame image as shown in Fig.2.

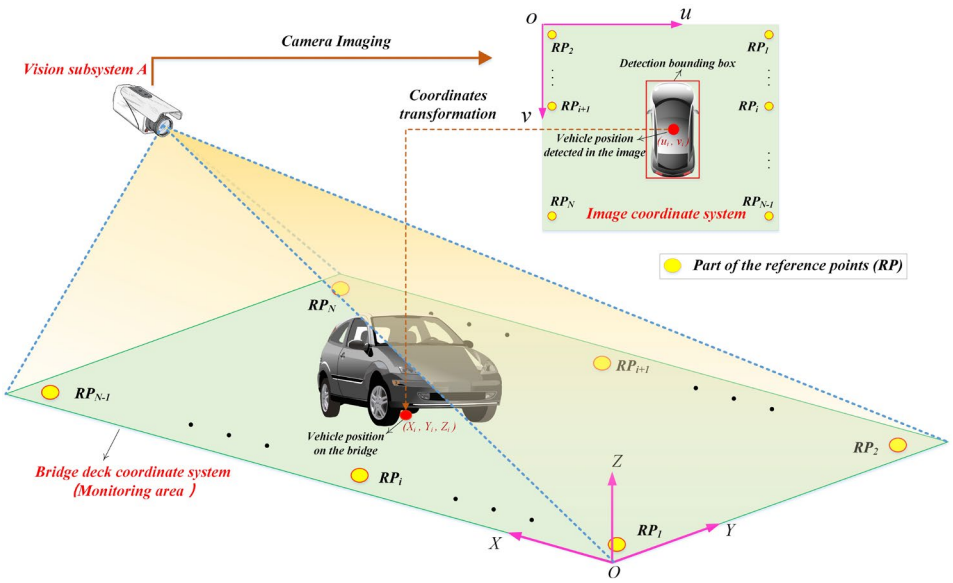

Fig.2 Explanation of the process of vehicle locating

For transforming an identified vehicle position in the image coordinates to the

bridge deck coordinates, the principle of projection geometry is used.

$$\begin{bmatrix} X_1 & Y_1 & Z_1 & 1 & 0 & 0 & 0 & 0 & -u_1X_1 & -u_1Y_1 & -u_1Z_1 \\ 0 & 0 & 0 & 0 & X_1 & Y_1 & Z_1 & 1 & -v_1X_1 & -v_1Y_1 & -v_1Z_1 \\ & & & \cdots & \cdots & \cdots & & & & & \\ & & & \cdots & \cdots & \cdots & & & & & \\ X_n & Y_n & Z_n & 1 & 0 & 0 & 0 & 0 & -u_nX_n & -u_nY_n & -u_nZ_n \\ 0 & 0 & 0 & 0 & X_n & Y_n & Z_n & 1 & -v_nX_n & -v_nY_n & -v_nZ_n \end{bmatrix} \times \begin{bmatrix} m_{11} \\ m_{12} \\ m_{13} \\ m_{14} \\ m_{21} \\ m_{22} \\ m_{23} \\ m_{24} \\ m_{31} \\ m_{32} \\ m_{33} \end{bmatrix} = m_{34} \begin{bmatrix} u_1 \\ v_1 \\ \cdots \\ \cdots \\ \cdots \\ \cdots \\ \cdots \\ \cdots \\ \cdots \\ u_n \\ v_n \end{bmatrix} \quad (1)$$

where (u_i, v_i) represents the image coordinates of reference points (i.e., yellow ellipses in Figure 2), (X_i, Y_i, Z_i) their corresponding bridge deck coordinates, and m_{ij} the element of the coordinate transformation matrix which is determined by the intrinsic and extrinsic camera parameters. By assuming $m_{34} = 1$, the unknowns m_{ij} can be solved by using the least squares method given the condition $n \geqslant 6$.

After the transformation matrix is determined, the bridge deck coordinates of the vehicle centre are calculable according to the corresponding image coordinates, and the vehicle trajectory can be measured by performing this operation on each image frame. In this process, image coordinates refer to centres of the detection bounding boxes of a designated side of the vehicle (top profile is chosen in this study). The advantage of this design is that it is beneficial to minimize identification errors of the vehicle centre image coordinates caused by changes in projection angle.

2.3 Computer Vision-based displacement measurement

Vision-based displacement measurement techniques are increasingly popular in SHM applications due to the non-contact nature of the measurement. In this study, a technique named gradient-based matching via voting (GMV) was used to measure

vehicle-induced displacement. The GMV technique was shown to be more robust and accurate in several indoor and outdoor tests under adverse effects of illumination changes and occlusions (Wang et al. 2022), in comparison with other available techniques, such as feature point matching (Dong and Catbas 2019), optical flow (Yoon et al. 2016) and template matching (Feng et al. 2017).

The GMV is an improved normalized cross-correlation-based technique using a voting strategy and the similarity of pixel gradients for feature tracking. The main steps of the GMV technique are given below:

Step 1: Calibration of intrinsic camera parameters; definition of the first video frame as the reference frame.

Step 2: In the reference frame, a region of interest (ROI) for the measurement target is selected. Edge points are extracted from the ROI to form a template, and the elements of the template are regarded as voters.

Step 3: In all subsequent frames, a voting process is conducted to calculate the similarity between the template and all possible areas of the same size as the template. The pixel displacement of the target can be determined as a peak position of the similarity score map.

Step 4: Interpolation for subpixel displacement estimations for better resolution; final conversion from the subpixel displacements into physical displacements.

2.4 Damage Localisation Using DILs

Using Maxwell's reciprocal theorem, a displacement influence line of a vehicle

loading is the displacement when the vehicle loading is applied to the displacement sensor location provided that the dynamic effect is negligible. Damage localisation by a DIL is effectively the same as damage localisation using static loading tests.

Inspired by the methods using static displacements from static loading tests or equivalent from modal flexibility matrices (Choi et al. 2004; K. Koo et al. 2011; Le et al. 2019), this paper applied damage-induced displacement influence line (DIDIL) to localise damages. As shown in Fig.3, a simply supported (SS) beam is taken as an example to illustrate the process of damage localisation.

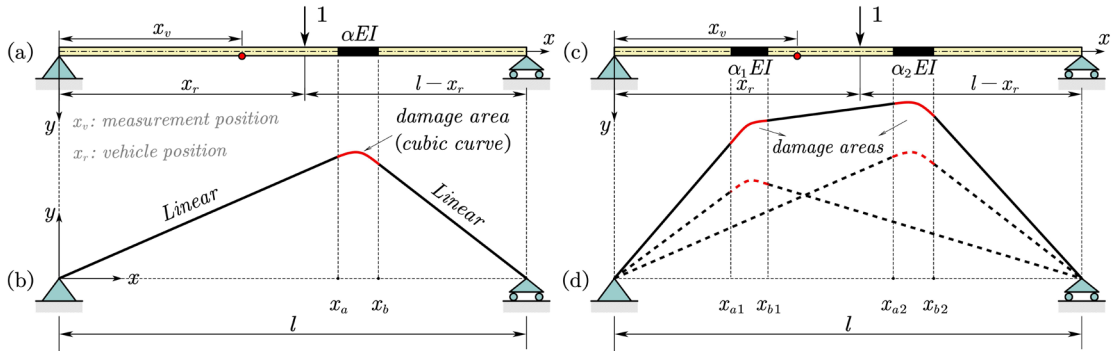

Fig.3 Damage-induced displacement influence lines: (a) single damaged beam; (b) DI-DIL of (a); (c) double damaged beam; (d) DI-DIL of (c).

As the moving load is measurable by using vision subsystem A and WIM system, only a single measurement point at x_v is necessary to measure DILs. According to the Principle of Virtual Work, the deflections of the intact and damaged (SS) beam at the measurement point under a unit load acting at the location x_r can be derived, i.e., generating DIL functions. The damage localisation index is defined by the damage-induced change in DILs, which is given as

$$DIDIL(x_r) = |y_D(x_r) - y_I(x_r)| \tag{2}$$

where $y_I(x_r)$ and $y_D(x_r)$ are the DIL values before and after damage.

For a single damage case, it can be proved that the indicator $DIDIL(x_r)$ appears linear in undamaged areas but it takes on a cubic curve with a maximum amplitude in the damaged area (i.e., Fig.3(a) and (b)). Based on this fact, damage is localised by the vertex point of a triangular shape of the damage-induced displacement influence line (DIDIL).

For scenarios with multiple damages, the *DIDIL* is, using the principle of superposition, a sum of several triangular DIDILs (i.e., Fig.3(c) and (d)). Multiple damages are localised by sharp corners where the slope of the piecewise linear curve of the damage-induced displacement influence line (DIDIL) changes abruptly.

While calculating DIDILs is theoretically straightforward, the quality of DIDILs in practical measurement is subject to various factors, such as the accuracy of vision systems, the precision of time synchronization, and changes in structural status. For example, the initial structural displacements in different loading tests may vary due to changes in the boundary friction effect, resulting in DILs drifting away from zero at the supports (x=0 and x=l). To compensate for such an effect, this study proposes a chordwise displacement approach as shown in Fig.4. DILs are substrated by the chord displacement connecting the two points of $y(x)$ at x=0 and x=l. Then the chordwise displacement (cwDIL) $y_{cw}(x)$ is guaranteed to be zero at the two supports.

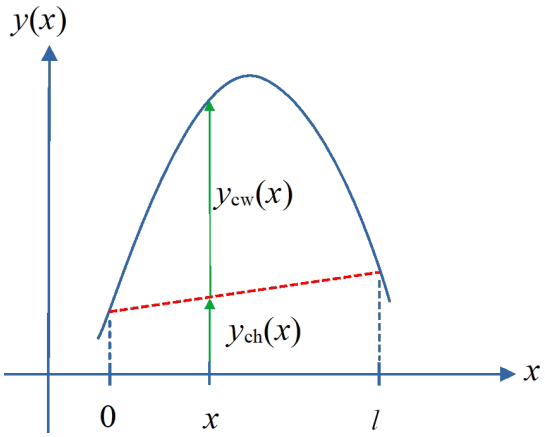

Fig.4 Chord-wise Displacement Influence Line

In addition, it is noteworthy that detecting sharp corners solely based on curvature at a single point may cause false positives due to noise interference in actual measurements of DIDILs. Therefore, for accurate automatic detection, it is beneficial to apply some corner detectors considering regional curvature change and contour features (He et al. 2017a; Zhang et al. 2022).

3 Laboratory experiment

3.1 Experiment setup and instrumentation

A laboratory experiment was carried out on a simply supported beam (Fig.5) to validate the DILs measured by Computer Vision. The test structure was made of a steel beam with dimensions of 2.49m×20cm×6mm. The support on the left was a hinge and the other on the right was a roller, with a distance between the supports of 2.16m.

For displacement measurement, two targets were mounted along the structure, while another one was fixed on the ground as a reference. The test structure was loaded with a two-axle moving vehicle. Guardrails were arranged on the upper surface of the bridge to prevent the vehicle from falling, and 39 reference points were evenly marked

for the calculation of transformation matrix as discussed in Section 2.2.

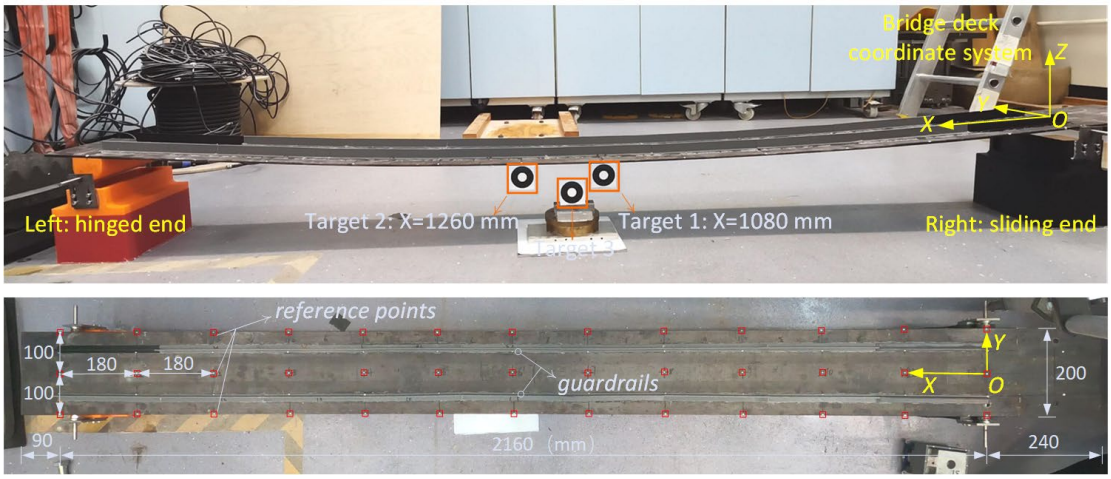

Fig.5 Test structure: (top) overview, and (bottom) top view

A model vehicle (Fig.6) with a weight of 2.05 kg was used as a moving load and was horizontally pulled along the structure from the right end to the left by a fishing wire. The advantage of this approach rather than using a motor pulling at a constant speed was the variability of the vehicle speed, which is close to real conditions on real bridges.

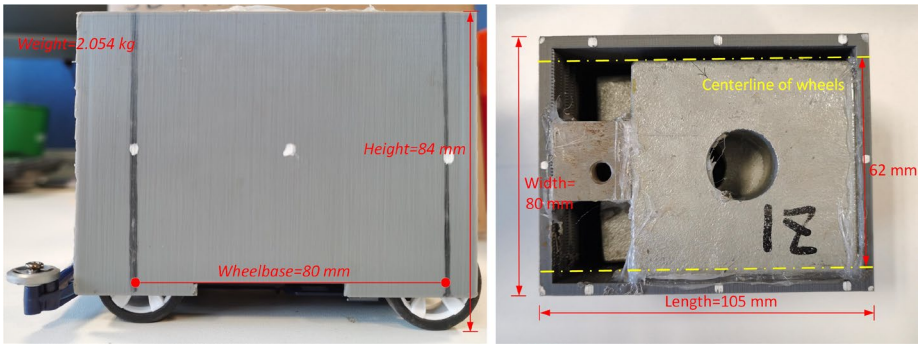

Fig.6 Model Vehicle

Both the position of the model vehicle and displacements of the structure were measured by the computer vision techniques discussed in Sections 2.2 and 2.3. Fig.7 shows the layout of the two cameras. A GoPro camera was installed above the beam to capture the vehicle position in the whole range of the bridge, while a single-lens reflex camera, of which the shooting direction was perpendicular to the beam axis, was

mounted on one side of the structure to measure vertical displacements of the two targets. Despite the proposed method only requiring the measurement of a single target measuring two targets is intended to compare the damage detectability of the DILs at different positions. The two cameras were synchronised by a sound made by a clapperboard. The sound signals were sampled at a high frequency (48kHz), which provides high synchronization accuracy when determining timestamp differences based on signal peak positions.

Fig.7 Layout of cameras for vehicle tracking and structural displacement measurement

3.2 Damage Scenarios

The test structure was stiffened with single or double steel plates attached beneath the beam, rather than damaged. The original structure can be regarded as damaged in comparison to the stiffened one. This approach enables the test structure to be reusable for any number of different damage scenarios.

Three types of steel plates (Fig.8) were attached at two positions, i.e., the damage centres 1 or 2 in Fig.9. Using different combinations of size and position of the steel

plates, five damage scenarios were considered as shown in Table 1.

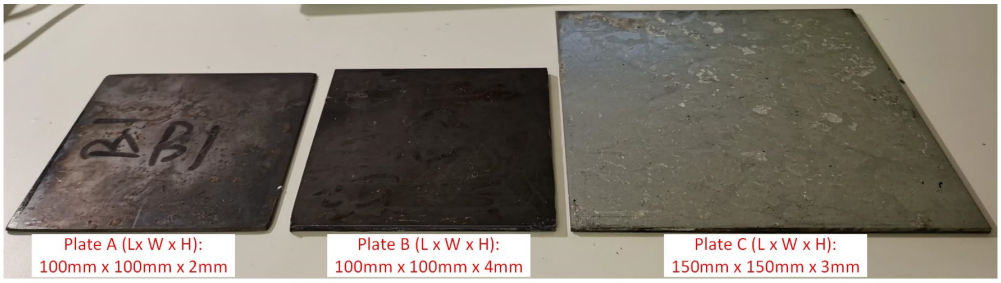

Fig.8 Steel plates used in the experiment: (left) Plate A, (middle) Plate B, and (right) Plate C

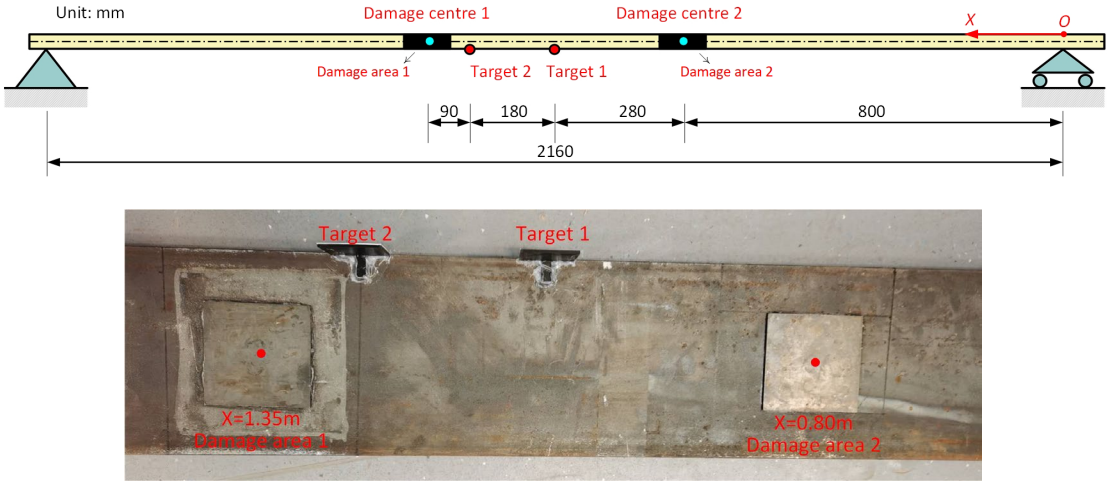

Fig.9 Positions of the damage areas relative to the targets: (upper) layout; and (bottom) photo

Table 1. Damage Scenarios

Damage scenarios	Positions	Plate types	Descriptions
Intact	--	--	No plate attached.
SD 1	Damage centre 1	Plate A	Small damage.
SD 2	Damage centre 1	Plate B	Medium damage.
SD 3	Damage centre 1	Plate C	Large damage.
DD	Damage centre 1 & 2	2 × Plate B	Double medium damages.

Notes: "*SD*" and "*DD*" represent "Single Damage" and "Double Damage", respectively.

For each damage scenario, the structure was loaded by the vehicle 12 times to observe repeatability of the experiment and a total of 60 DILs for the 5 damage scenarios were measured.

3.3 Displacement Influence Line Measurements

In order to get a DIL from each experiment, the raw measurements of the vehicle position and CV-based displacement of the structure need to be obtained first, and then fused with a proper time-synchronisation.

For vehicle position measurements, the YOLO-v4-based model and Kalman filtering algorithm were used to detect and track the vehicle. The YOLO-v4-based model was trained with 1834 annotated images captured by the vision subsystem *A* as shown in Fig.10(a). The forces acting on the bridge were simplified to a single-point load at the centre of the detected bounding box. According to Eq.(2), the image coordinates of the single point load were converted to actual positions on the structure. Since the structural deflection under the self-weight was too large to be ignored, the elevation change of the bridge deck was considered in the coordinate transformation. Fig.10(b) & (c) show the 24 curves of vehicle position and vehicle speed in damage cases "*Intact*" and "*SD*3". Fig.10(b) shows that the vehicle was placed on a point before the right support (the negative x coordinate at t=0), and started to move to the left. However, due to a configuration problem of the vehicle camera, the vehicle location was tracked only up to a point just before the left support at x=216 cm. Fig.10(b) showed that the vehicle speed varied significantly in the range of 0-0.5 m/s, which was different from the speed patterns reported in previous studies.

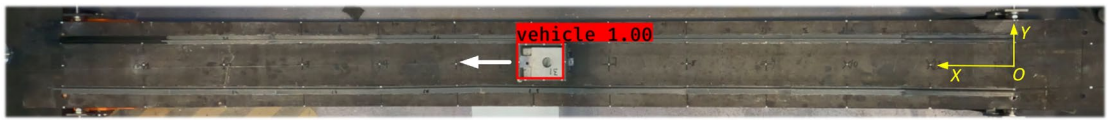

(a)

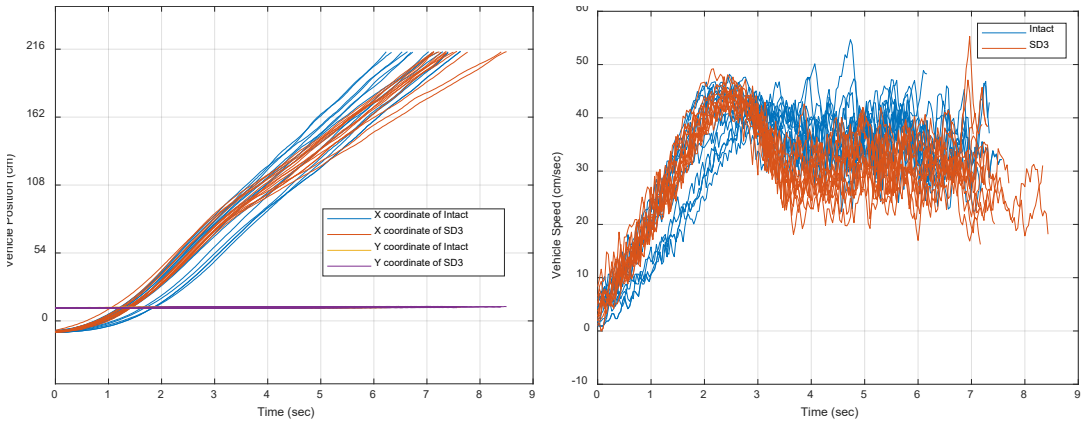

(b) (c)

Fig.10 Input loading identification: (a) vehicle detection; (b) vehicle position time history; (c) vehicle speed time history

Fig.11 presents the FOV of subsystem B. To compare the damage detectability of the identified DILs at different positions, two measurement targets were used in this study. Despite this, it should be noted that the single-target measurement is optimal for DIL-based damage detection, which provides better precision of displacements.

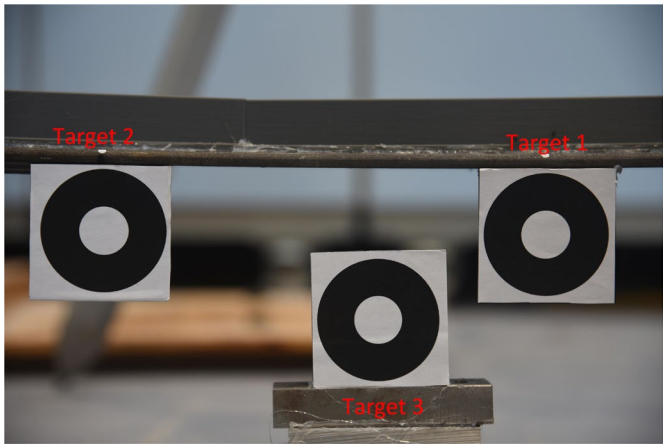

Fig.11 Targets captured by vision subsystem B for displacement measurements

For CV-based displacement measurements of the structure, the GVM method was applied to the videos from vision subsystem *B*. Fig.12 shows a typical time history in damage cases "*Intact*" and "*SD2*". It is worth noting that point *A* presents the time when

the model vehicle was placed on the structure, point *B* the time when the model vehicle started to move, and point *C* the time when the model vehicle left the structure followed by a free vibration of the structure. It can be seen that the displacement amplitudes were clearly reduced in the damage case "*SD2*", showing the stiffening effect.

Fig.12 shows two interesting observations: 1) the displacement of Target 1 in "SD2" didn't start from zero and 2) the displacements of Target 3 in both "Intact" and "SD2" were slightly off from zero. The former observation indicates that the friction effect on the supports prevented the structure from being restored to the initial displacement before vehicle loading. The latter observation indicates that the CV-based displacement measurements had a drift that was likely caused by the gradual tilt of the camera mounting due to the gravitational effect of the lens. The former effect by friction was found to be significantly larger than the latter effect. Fig.13 presents the displacement of Target 3 during the twelve runs of measurements. It is seen that although the camera tilting is visible but occurs at a slow rate, rendering it negligible during a single run that typically lasts a few seconds.

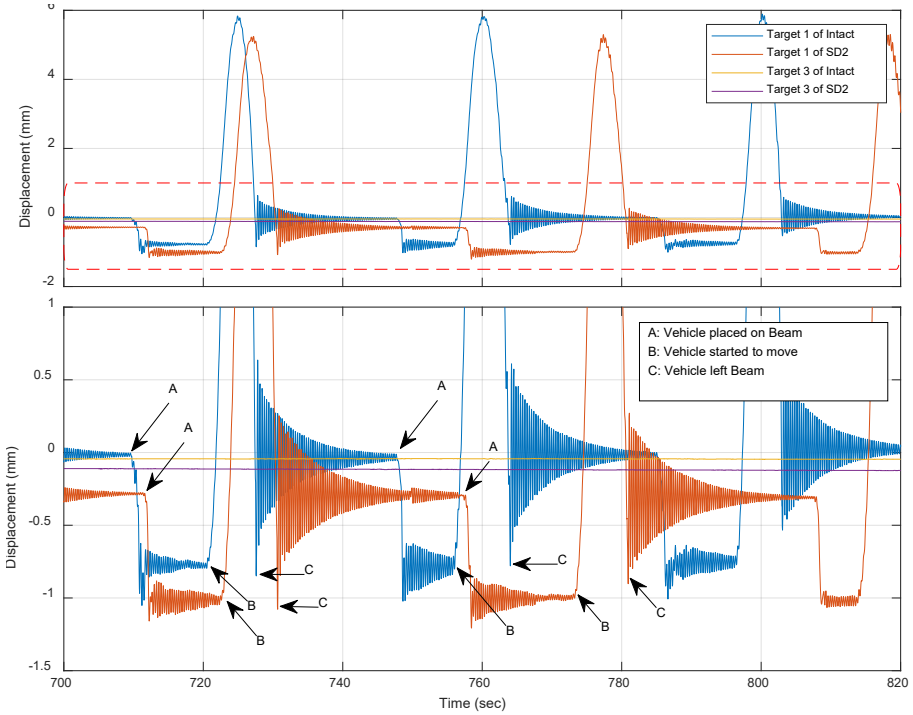

Fig.12 CV-based displacement measurements of Targets 1 and 3: (top) Overview, (bottom) Zoomed View

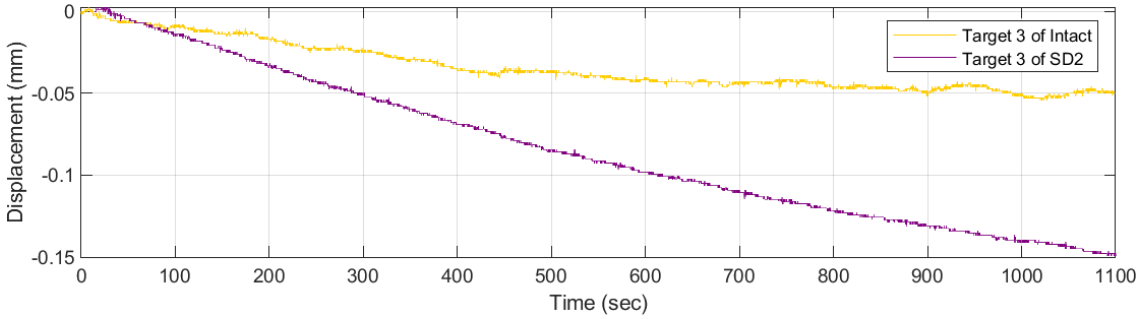

Fig.13 Displacement of Target 3 during continuous measurements

For constructing a DIL from the two measurements obtained above, the following three steps were used: 1) the timestamps of the vehicle position and displacement were aligned using the recorded audio signals; 2) the dynamic component of the vehicle-induced displacement was low-pass filtered to get a quasi-static displacement as shown in Fig.14. The cut-off frequency was 1.5 Hz while the first frequency of the structure was about 3.15 Hz; 3) the time history of the static displacement and the corresponding

vehicle trajectory were fused to generate a quasi-static displacement influence line.

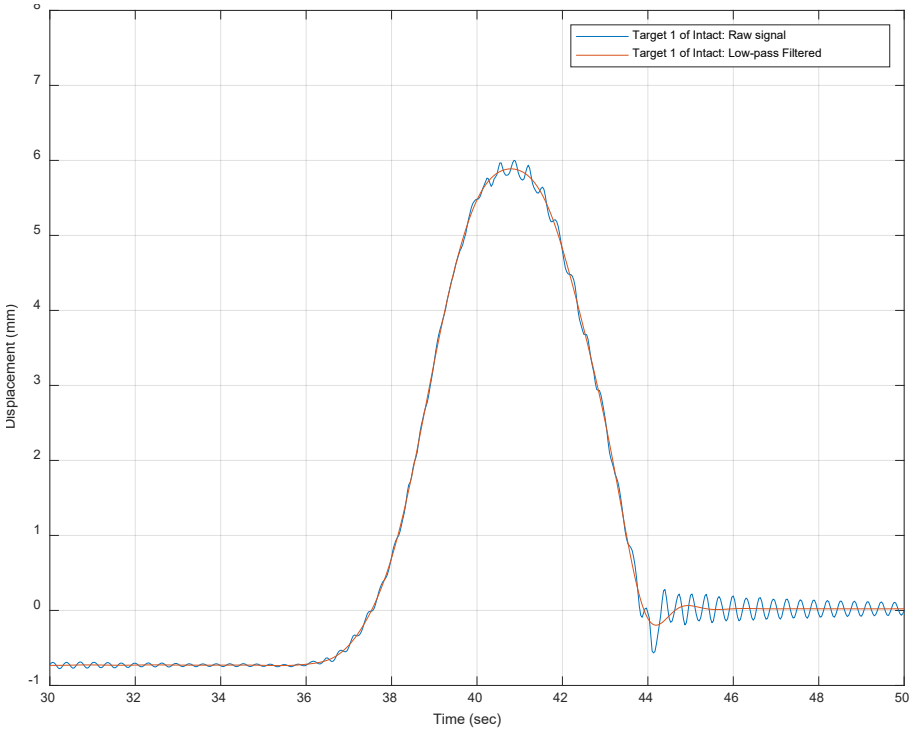

Fig.14 Static component of vehicle-induced displacement by a low-pass filtering

DILs from different tests were standardized to the same size using spline interpolation and resampling to facilitate averaging and standard deviation calculation. The averaged DILs of Targets 1 & 2 for the "*SD2*" case are shown in Fig.15 with 2.5σ deviation levels from 12 repeated tests.

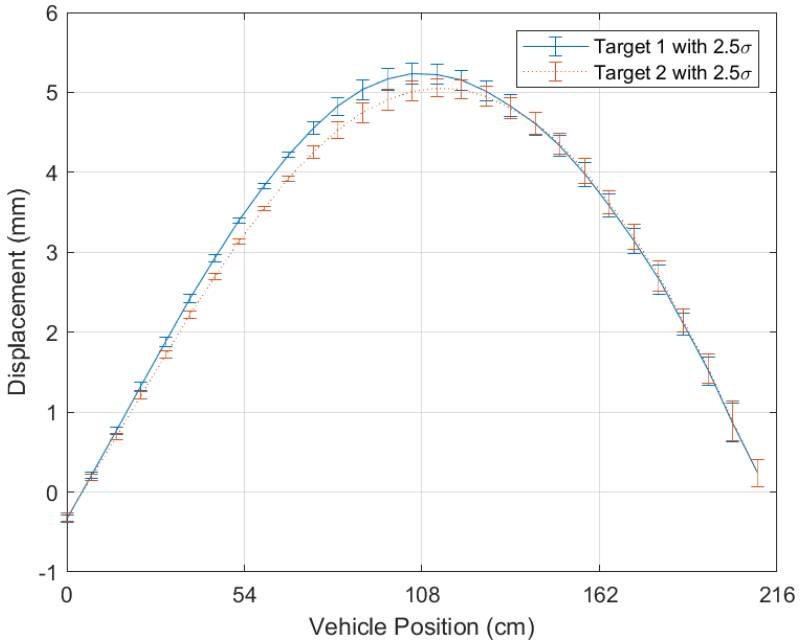

Fig.15 Static DILs of Targets 1 & 3 with 2.5σ deviation levels

It is worth noting that the displacements at the left end $x(0)$ were below 0, which was mainly caused by the friction effect of the bearings. To compensate for such effects, the chordwise displacement approach introduced in Section 2.4 was applied. The chordwise DILs from Targets 1 & 3 are shown in Fig.16, in which they are compensated to be zero at x=0 and x=209.5 cm that was the maximum coordinate tracked as shown in Fig.10(b). In Fig.16, the largest standard deviation of the DILs at Targets 1 and 2 are 0.073mm and 0.078mm, indicating comparable accuracy with a state-of-art approach to vision-based displacement measurements (Martini et al. 2022). The precision of displacement can be further improved by increasing target image size, e.g., by performing single-point measurement.

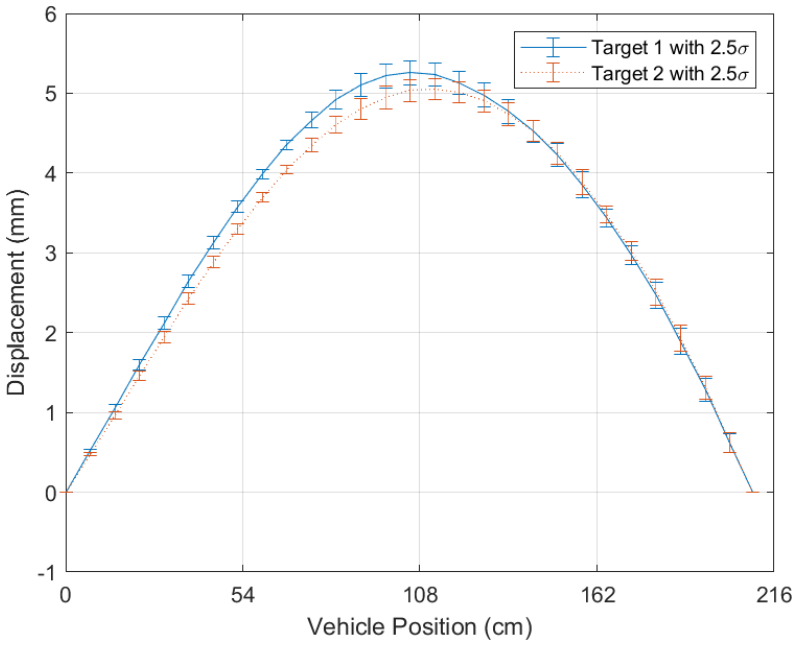

Fig.16 Chord-wise Displacement Influence Lines of Targets 1 & 3 with 2.5σ deviation levels

Furthermore, it should be noted that the deviation of DILs was not only from displacement measurement, but also from errors in vehicle localization. Since the displacement is analytically a function of loading position, errors in vehicle localization may introduce additional variability into the measured DILs. Regarding this, the 1834 annotated images, which were also from the "*SD2*" case, were used as ground truth for error analysis. Fig.17 shows the mean error and standard deviation of the vehicle localization at different positions along the bridge model. It is seen that the proposed system achieved stable and highly accurate measurements of vehicle position.

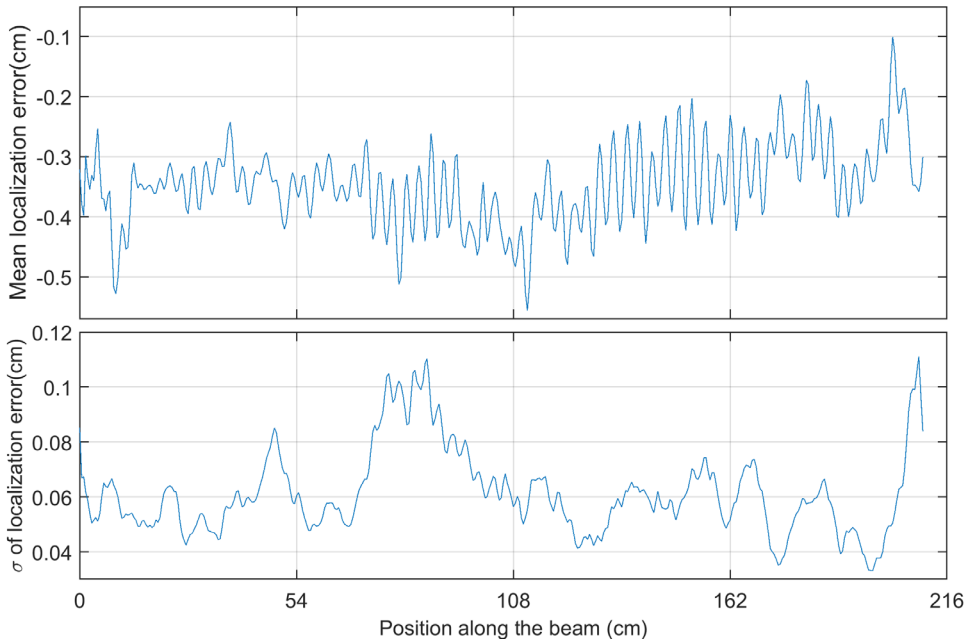

Fig.17 Error analysis for vehicle localization: (top) mean error; (bottom) standard deviation

This section has shown that the proposed vision systems have high accuracy in both vehicle position and displacement measurements. However, it should be explained that the standard deviation of DILs, which is illustrated in Fig.15 and Fig.16, increases with the vehicle position. This trend was also reported in a recent study (Martini et al. 2022) and was possibly caused by changes in lighting conditions. Reduction in brightness may lead to a gradually increasing bias in the displacement. Therefore, proper illumination compensation is also beneficial to improve vision-based displacement measurement.

3.4 Damage Detection Results

12 DILs for each damage scenario were obtained by fusing the two CV-based measurements. Damage-induced changes in the DILs before and after damage were investigated and presented in the section.

Fig.18(a) shows the chordwise displacement influence lines with 2.5σ deviation levels of Target 1 for the damage case "SD3" from "Intact". Fig.18(b) shows a zoomed view of the damage-induced chordwise DIL together with the location of the damage centre 1. It clearly shows that the damage-induced cwDIL is significantly larger than the 2.5 σ of the cwDIL of "SD3", indicating a statistically significant detection of the damage. Also, the damage is shown successfully localised by the maximum point in the damage-induced cwDIL.

Fig.18(c&d) and (e&f) show the results for the smaller damage cases: "SD2" from "Intact", and "SD1" from "Intact", respectively. As shown in Fig.18(d) and (f), the damage existence detections are successful beyond the 2.5σ deviation levels for both cases. Damage localisation is also successful by the maximum points in the damage-induced cwDILs.

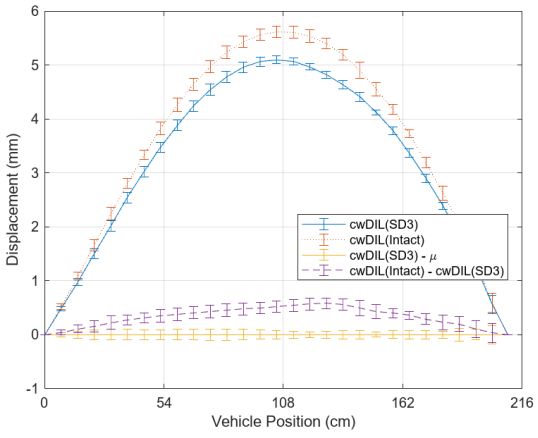

(a)

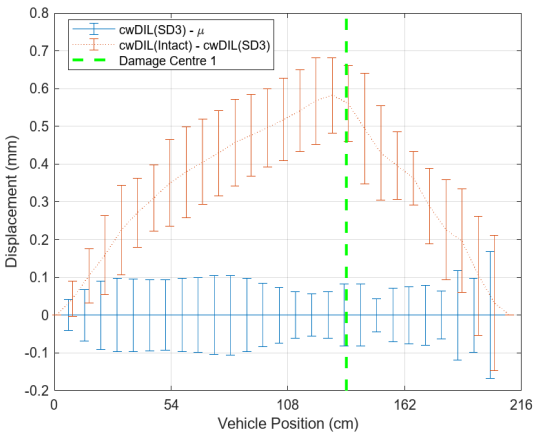

(b)

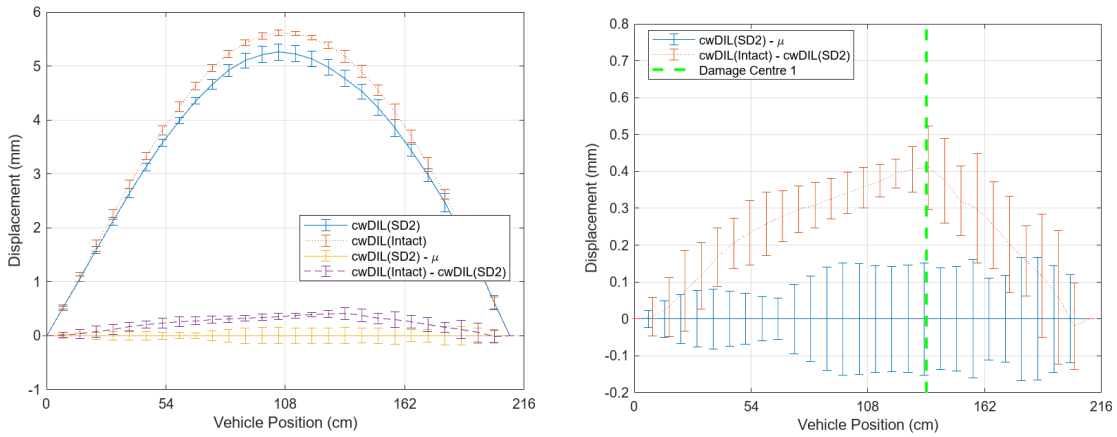

(c) (d)

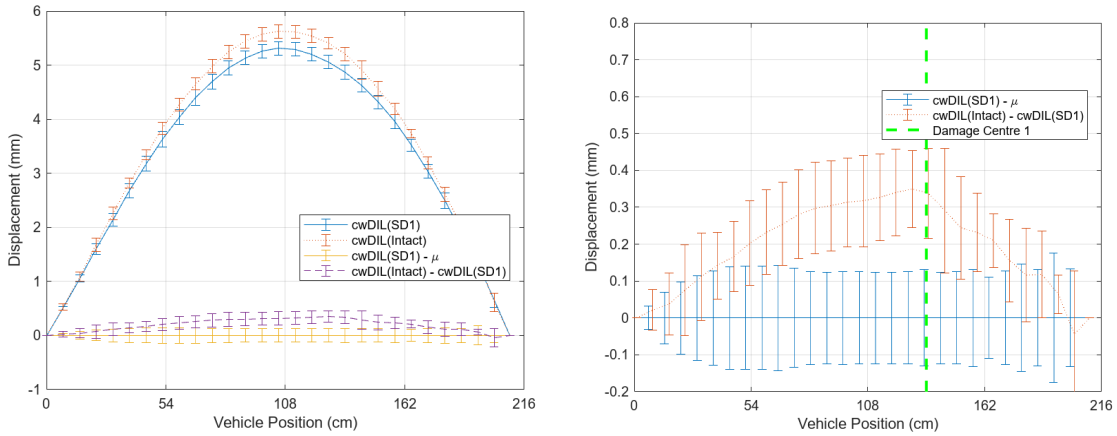

(e) (f)

Fig.18 Chordwise DILs with 2.5σ and the damage-induced change from Target 1: (a & b) SD3; (c & d) SD2; (e & f) SD1

Fig.19 presents the damage detection results for the cases with "DD". Fig.19(a&b) show the cwDILs for damage case "DD" from "Intact", and the corresponding damage-induced change. The damage-induced cwDIL is large enough beyond the 2.5 σ deviation levels of damage case "DD" and two damage centres were localised by the slope changing points of the piecewise linear curve. Fig.19(c&d) show the cwDILs for damage case "DD" from "SD2", and their damage-induced change. The difference between the two cases was the restrengthening in damage area 1, which was in effect a single damage case. It was found that the damage was marginally detected by the

damage-induced cwDIL just beyond the 2.5 σ deviation levels of damage case “SD2” and was localised correctly by the damage centre 1.

Fig.20 shows the damage-induced cwDILs obtained from Target 2. By comparing Fig.20(a) with Fig.18(b), it was found that the damage-induced cwDIL in Fig.20(a) was larger than that in Fig.18(b). This observation can be explained by the fact that Target 2 was closer to the damage centre 1 than Target 1 as shown in Fig.9. Similarly, Fig.20 (b) shows a smaller damage-induced cwDIL than that in Fig.18(f) as Target 2 was further away from the damage centre 2 than Target 1.

The damage-induced cwDIL shown in Fig.20(b) was close to the smallest damage this experiment was able to detect over the 2.5 deviation levels (about 0.16mm). For better damage detection sensitivity, it is required to measure cwDILs with smaller deviation levels.

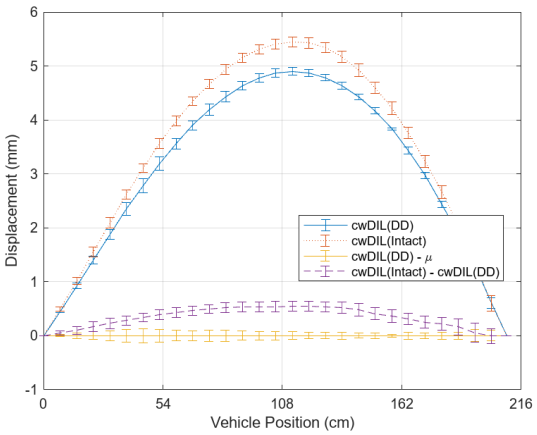

(a)

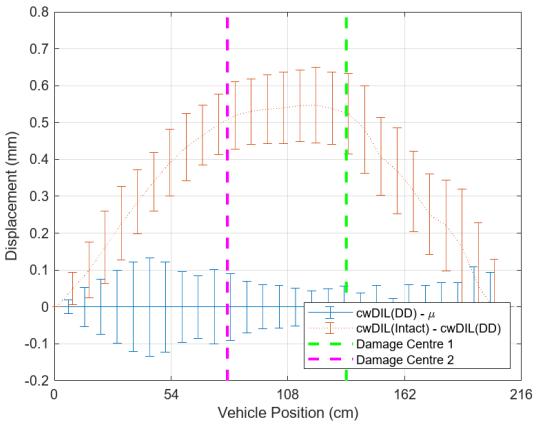

(b)

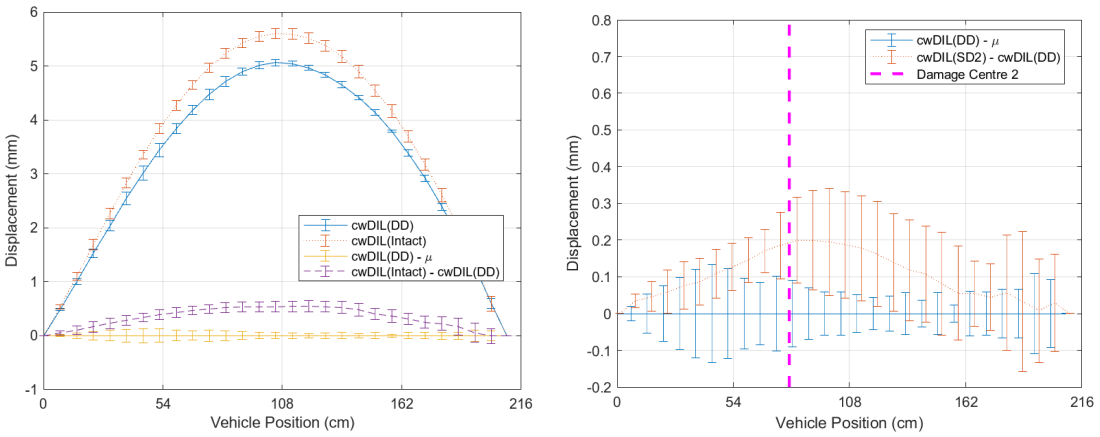

(c) (d)

Fig.19 Chordwise DILs with 2.5σ and their amagedged-induced change from Target 1: (a & b) DD from Intact; (c & d) DD from SD2

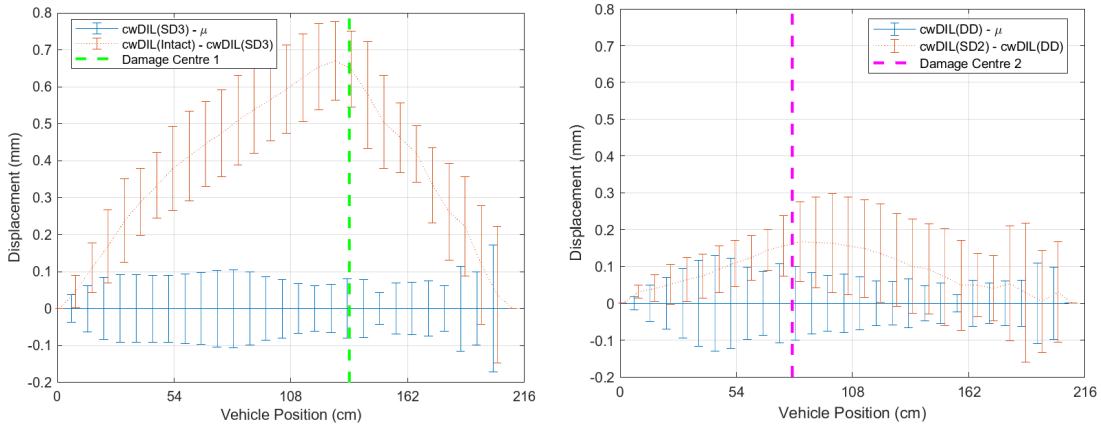

(a) (b)

Fig.20 Changes in chordwise DILs from Target 2: (a) SD3 from Intact; (b) DD from SD2

3.5 Discussion

The results provided evidence that the proposed CV-based DILs using the chordwise approach were consistently successful for both damage existence detection and localisation for all single and double damage cases, in the existence of different vehicle speeds. However, since this paper only presents preliminary laboratory results, there are still some gaps between the proposed approach and practical applications. Some discussion and suggestions for filling in these gaps are given below.

(1) It was found that friction on the supports can defend the structure from restoring and deviate DIL measurements. While the chordwise approach effectively compensated friction effects in this study, understanding the friction mechanism under more complex boundaries and their reduction still remain to be explored.

(2) Fig.15 revealed greater deviations around the left support as compared to the right support, which was possibly due to the lighting changes during the displacement measurement process. Therefore, improving camera imaging quality with illumination compensation and higher resolution can potentially improve damage detection sensitivity.

(3) For a clearer illustration, the maximum displacement presented in this study is around 6mm, which corresponds to 1/360 of the main span. This deflection-span ratio is relatively large for real bridges. However, it is reasonable to assume that the bridge model behaved elastically during the tests since the applied load remained far below the ultimate design capacity and no plastic deformation was detected. Moreover, compared to striving for consistency in the deflection-span ratio, achieving adequate DIL resolution is more important for practical measurements.

(4) Although the proposed vision-based subsystems have shown high precision in DIL measurement and the potential to continuously detect damage for operational bridges, the current investigation is limited to laboratory conditions. Unlike the test bridge, real bridges have more complex boundaries, smaller damages, are subject to various environmental factors (e.g. temperature), and are even made of other

materials (e.g, concrete). Therefore, the performance of the proposed vision-based damage detection framework on a bridge under more realistic conditions remains to be further studied in the future.

4 Conclusion

This study presented a feasibility study on an input-output vision-based system to measure displacement influence lines for applications of bridge damage detection. The feasibility has been validated through a series of laboratory experiments on the simply supported beam model. Some conclusions can be summarized as follows.

- The vision-based system showed high precision in measuring vehicle position and displacement, leading to accurate displacement influence lines (DILs). Through experimental studies on the laboratory test structure, the measured DILs were found to effectively assess the existence and location of damages. The damage detection and localisation were carried out successfully for all 5 damage scenarios consistently.
- The Chordwise Displacement Influence Line (cw-DIL) was proposed to compensate adverse effects of friction in the boundary supports and was shown effective through successful damage detection and localisation results. Even so, it is noteworthy that for more complex adverse effects, such as thermal effects and camera imaging errors, the current compensation method may require further improvement.
- The proposed DIL-based damage detection approach was successfully validated

using random vehicle speeds while a novel concept of integrating the WIM system with dual-vision systems was suggested, which provides insights into the possibility of continuous damage detection in operational bridges under normal traffic.

- The quality of DIL measurements significantly influences damage detectability. In this study, the maximum standard deviation of measured DILs was under 0.08mm, while the smallest detectable damage-induced displacement, considering 2.5 deviation levels, was approximately 0.16mm. To balance accuracy and sensitivity in damage detection, it is recommended to maintain the maximum standard deviation at no more than half of the target damage-induced displacement.

Although this study obtained promising results for damage detection in a test bridge, there are many aspects to be further developed and validated in the existence of ambient environmental changes, boundary frictions, and nonlinearities existing in the field condition.

Acknowledgement

This study is financially supported by the Fundamental Research Funds for the Central Universities (20210205), the Zhejiang Zhoushan Sea-crossing Bridge Co Ltd. in the project “Vortex Vibration Prediction Technology of Xihoumen Bridge”, the China Railway Siyuan Survey and Design Group Co., Ltd. in the project "Research on the Target System and Index Algorithm of Urban Cluster Bridge Monitoring" (2020K-006-

1), the National Natural Science Foundation of China(51878490), and the CSC (China Scholarship Council) Scholarship (202006260246).

References

Breccolotti, M., &Natalicchi, M. (2022). Bridge damage detection through combined quasi-static influence lines and weigh-in-motion devices. *International Journal of Civil Engineering, 20*(5), 487-500.

Brownjohn, J., Bocciolone, M., Curami, A., Falco, M., &Zasso, A. (1994). Humber bridge full-scale measurement campaigns 1990–1991. *Journal of Wind Engineering and Industrial Aerodynamics, 52*, 185-218.

Chen, Z., Cai, Q. L., &Zhu, S. (2018). Damage quantification of beam structures using deflection influence lines. *Structural Control and Health Monitoring, 25*(11), e2242.

Chen, Z., Yang, W., Jun, L., Cheng, Q., &Cai, Q. (2017). A systematic method from influence line identification to damage detection: Application to RC bridges. *Computers and Concrete, An International Journal, 20*(5), 563-572.

Choi, I.-Y., Lee, J. S., Choi, E., &Cho, H.-N. (2004). Development of elastic damage load theorem for damage detection in a statically determinate beam. *Computers & Structures, 82*(29-30), 2483-2492.

Cross, E., Koo, K., Brownjohn, J., &Worden, K. (2013). Long-term monitoring and data analysis of the Tamar Bridge. *Mechanical Systems and Signal Processing, 35*(1-2), 16-34.

Dan, D., Yu, X., Han, F., &Xu, B. (2022). Research on dynamic behavior and traffic management decision-making of suspension bridge after vortex-induced vibration event. *Structural Health Monitoring, 21*(3), 872-886.

Das, S., Saha, P., &Patro, S. (2016). Vibration-based damage detection techniques used for health monitoring of structures: a review. *Journal of Civil Structural Health Monitoring, 6*(3), 477-507.

de Battista, N., Brownjohn, J. M., Tan, H. P., &Koo, K.-Y. (2015). Measuring and modelling the thermal performance of the Tamar Suspension Bridge using a wireless sensor network. *Structure and Infrastructure Engineering, 11*(2), 176-193.

Doebling, S. W., Farrar, C. R., Prime, M. B., &Shevitz, D. W. (1996). Damage identification and health monitoring of structural and mechanical systems from changes in their vibration characteristics: a literature review.

Dong, C., Bas, S., &Catbas, F. N. (2019). A completely non-contact recognition system for bridge unit influence line using portable cameras and computer vision. *Smart Structures and Systems, An International Journal, 24*(5), 617-630.

Dong, C., &Catbas, F. N. (2019). A non-target structural displacement measurement method using advanced feature matching strategy. *Advances in Structural Engineering, 22*(16), 3461-3472.

Erdenebat, D., &Waldmann, D. (2020). Application of the DAD method for damage localisation on an existing bridge structure using close-range UAV photogrammetry. *Engineering Structures, 218*. doi:10.1016/j.engstruct.2020.110727

Feng, D., Scarangello, T., Feng, M. Q., &Ye, Q. (2017). Cable tension force estimate using novel noncontact vision-based sensor. *Measurement, 99*, 44-52.

Ge, L., Dan, D., Koo, K. Y., &Chen, Y. Long-term monitoring system for full-bridge traffic load distribution on long-span bridges.

Ge, L., Dan, D., &Li, H. (2020). An accurate and robust monitoring method of full‐bridge traffic load distribution based on YOLO‐v3 machine vision. *Structural Control and Health Monitoring, 27*(12), e2636.

Han, Q., Ma, Q., Xu, J., &Liu, M. (2021). Structural health monitoring research under varying temperature condition: a review. *Journal of Civil Structural Health Monitoring, 11*(1), 149-173.

He, W., Ren, W., &Zhu, S. (2017a). Baseline-free damage localization method for statically determinate beam structures using dual-type response induced by quasi-static moving load. *Journal of Sound and Vibration, 400*, 58-70. doi:10.1016/j.jsv.2017.03.049

He, W., Ren, W., &Zhu, S. (2017b). Damage detection of beam structures using quasi-static moving load induced displacement response. *Engineering Structures, 145*, 70-82.

Huseynov, F., Kim, C., Obrien, E. J., Brownjohn, J., Hester, D., &Chang, K. (2020). Bridge damage detection using rotation measurements–Experimental validation. *Mechanical Systems and Signal Processing, 135*, 106380.

Khuc, T., &Catbas, F. N. (2018). Structural Identification Using Computer Vision–

Based Bridge Health Monitoring. *Journal of Structural Engineering, 144*(2). doi:10.1061/(asce)st.1943-541x.0001925

Koo, K.-Y., Brownjohn, J., List, D., &Cole, R. (2013). Structural health monitoring of the Tamar suspension bridge. *Structural Control and Health Monitoring, 20*(4), 609-625.

Koo, K., Sung, S.-H., &Jung, H.-J. (2011). Damage quantification of shear buildings using deflections obtained by modal flexibility. *Smart Materials and Structures, 20*(4), 045010.

Kromanis, R. (2021). *Characterizing Footbridge Response from Cyclist Crossings with Computer Vision-Based Monitoring.* Paper presented at the Civil Structural Health Monitoring: Proceedings of CSHM-8 Workshop.

Le, N. T., Thambiratnam, D., Nguyen, A., &Chan, T. (2019). A new method for locating and quantifying damage in beams from static deflection changes. *Engineering Structures, 180*, 779-792.

Lydon, D., Lydon, M., Kromanis, R., Dong, C. Z., Catbas, N., &Taylor, S. (2021). Bridge Damage Detection Approach Using a Roving Camera Technique. *Sensors (Basel), 21*(4). doi:10.3390/s21041246

Lydon, D., Lydon, M., Taylor, S., Del Rincon, J. M., Hester, D., &Brownjohn, J. (2019). Development and field testing of a vision-based displacement system using a low cost wireless action camera. *Mechanical Systems and Signal Processing, 121*, 343-358. doi:10.1016/j.ymssp.2018.11.015

Martini, A., Tronci, E. M., Feng, M. Q., &Leung, R. Y. (2022). A computer vision-based method for bridge model updating using displacement influence lines. *Engineering Structures, 259*, 114129.

Sohn, H., Farrar, C. R., Hemez, F. M., &Czarnecki, J. J. (2002). A Review of Structural Health Review of Structural Health Monitoring Literature 1996-2001.

Wang, M., Ao, W. K., Bownjohn, J., &Xu, F. (2022). A novel gradient-based matching via voting technique for vision-based structural displacement measurement. *Mechanical Systems and Signal Processing, 171*, 108951.

Xu, Y., Brownjohn, J., &Kong, D. (2018). A non-contact vision-based system for multipoint displacement monitoring in a cable-stayed footbridge. *Structural Control and Health Monitoring, 25*(5). doi:10.1002/stc.2155

Yoon, H., Elanwar, H., Choi, H., Golparvar‐Fard, M., &Spencer Jr, B. F. (2016). Target‐free approach for vision‐based structural system identification using consumer‐grade cameras. *Structural Control and Health Monitoring, 23*(12), 1405-1416.

Zaurin, R., &Catbas, F. (2009). Integration of computer imaging and sensor data for structural health monitoring of bridges. *Smart Materials and Structures, 19*(1), 015019.

Zaurin, R., &Catbas, F. N. (2011). Structural health monitoring using video stream, influence lines, and statistical analysis. *Structural Health Monitoring, 10*(3), 309-332.

Zaurin, R., Khuc, T., &Catbas, F. N. (2016). Hybrid sensor-camera monitoring for

damage detection: case study of a real bridge. *Journal of Bridge Engineering, 21*(6), 05016002.

Zhang, Y., Zhong, B., &Sun, X. (2022). *Corner Detection Based on a Dynamic Measure of Cornerity.* Paper presented at the PRICAI 2022: Trends in Artificial Intelligence: 19th Pacific Rim International Conference on Artificial Intelligence, PRICAI 2022, Shanghai, China, November 10–13, 2022, Proceedings, Part III.

Zhou, Y., Di, S., Xiang, C., Li, W., &Wang, L. (2018). Damage identification in simply supported bridge based on rotational-angle influence lines method. *Transactions of Tianjin University, 24*(6), 587-601.

Zhou, Y., Pei, Y., Li, Z., Fang, L., Zhao, Y., &Yi, W. (2020). Vehicle weight identification system for spatiotemporal load distribution on bridges based on non-contact machine vision technology and deep learning algorithms. *Measurement, 159*, 107801.